Exploring combined influences of material topography, stiffness and chemistry on cell behavior at biointerfaces

Zhou, Qihui

CHAPTER THREE

DIRECTING MESENCHYMAL STEM CELLS WITH GOLD NANOWIRE ARRAYS

Qihui Zhou, Zhiyuan Zhao, Ziwei Zhou, Gang Zhang, Ryan C. Chiechi*, Patrick van Rijn*

Advanced Materials Interfaces, 2018, 1800334

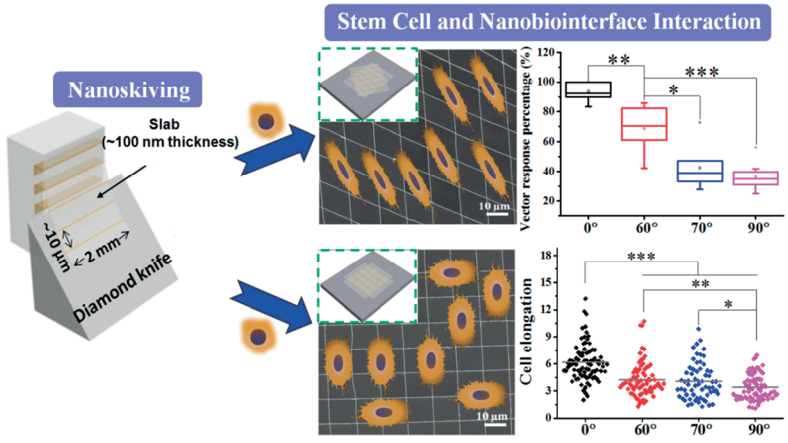

ABSTRACT

Controlling cell organization is still a major bottleneck in biointerface engineering when the material dimensions decrease to the nanoscale. Here Au nanowire-patterned array platforms with multi-scale design from the macroscale to the nanoscale are developed for studying human bone marrow-derived mesenchymal stem cell (hBM-MSC) response. When the angle of the Au nanowires on glass is increased from 0° to 90°, hBM-MSC arrangement exhibits a transition from a unidirectional distribution induced by a vector response to a bimodal polarization pattern. The degree of cell vector response and elongation decrease with increasing nanowire angles from 0 to 90°. Further, we demonstrate that the specific cell adhesion and organization are dependent on the surface micro/nanotopography, which is greatly enhanced by introducing stem cell-material affinity differences. This work provides an ideal model and new insights into a deeper understanding of cell-nanobiointerface interactions.

3.1. INTRODUCTION

Highly organized cellular systems such as tissues and organs, depend on appropriate microenvironmental cues, which comprise (bio)chemical signals as well as physical cues. Moreover, 'cells' have the unique capacity to adapt to changes in microenvironment and therefore physicochemical cues can be exploited to drive stem cell differentiation and function [1–5]. For any cell at an interface be it implants, tissue scaffolds for tissue engineering, or stimulation of cells into a defined functional state, perfect control with minimal input is desired as it all starts with the initial adhesion. Cell adhesion and organization are the first and critical cellular responses being influenced by cues including: composition, topography, elasticity, and biochemical signals. Cell organization precedes other cellular events such as migration direction, recruitment, differentiation, extracellular matrix (ECM) (re)organization and tissue functions [6–8]. In particular, cells from many tissues display aligned morphology, e.g., tendon cells [7], bone cells [9], and vascular smooth muscle cells [8] which is mediated by the ECM, which is often mimicked to achieve the same control via synthetic approaches.

To understand and control the cell organization, significant efforts have been made in the design and fabrication of biointerfaces with solely control of the surface topography, chemistry, and mechanical cues. The commonly used approach is to prepare surfaces with directional micro/nanotopography, such as aligned fibers [8], wrinkles [6,10,11], and grooves [12], on which cells align. Another approach is to design micro-patterned (bio)chemical cues with optimized sizes and cell-adhesive coatings on the surface. Cells prefer to adhere and align initially on the cell-adhesive materials due to the (bio)chemical and steric confinement, and subsequently spread to cell-repellent areas [13,14]. In the past decades, it has been demonstrated that cells are sensitive to isotropic or rough physicochemical structures (e.g., pits, islands, pillars, protrusions, dots) from the microscale to the nanoscale, and even atomic surface structure. For instance, some researchers reported that cells on microscale rough surface (Ra ≈ 1-2 μm) showed the strongest expression of osteogenic markers [15]. Dalby *et al.* and Zouani *et al.* reported that nanofeatures (nanopits and islands) of only 10 nm promoted cell adhesion and stimulated more filopodia generation [16,17]. Recently, Dong *et al.* demonstrated that the fate of hMSCs can be regulated by atomic scale surface roughness features of 5.7 Å which promoted differentiation while pluripotency was maintained with roughness features of 6.1 Å [18]. However, for anisotropic or aligned topographical structures, reducing the topography or dimensions of chemical patterns of biomimetic features to the nanoscale only exacerbates the problem of loss of specific adhesion and orientation. As a result, the effect of complex anisotropic patterns on cell organization is extremely challenging. Thus, there is a need for an accessible, efficient and flexible platform to study and affect cell organization for biomedical applications; the lack of a versatile and easy-to-use platform to prepare advanced, nanopatterned surfaces with precise control over size, spacing, pattern, and chemical cues hampers advancement in this field, in particular without the need of (bio)chemical modifications.

To address the challenge, we report herein that difference in affinity of cells towards non-modified materials combined with complex nanotopographical feature formation using nanoskiving, is able to direct cell morphology. Utilizing the surface micro/nanotopography and cell-material affinity difference, we developed the nanowire-array vector alignment of cells (NAVAC) approach. As two directions

combine as a vector, human bone marrow-derived mesenchymal stem cells (hBM-MSCs) sense this vector and align accordingly, which is termed the cell vector response. The nanotopography alone, gold nanowires on gold substrate, already showed to influence cell directionality. However, introducing the difference in materials affinity, gold nanowires on glass, the lower affinity enhanced the topographical cues and thereby facilitates cell morphology control. This approach is a bio-mimicking nanotopography tool that affects effective cell adhesion and orientation and control over cell spreading while maintaining cell orientation using a vector response introduced by differently oriented overlaying gold nanopatterns.

3.2. RESULTS AND DISCUSSION

The fabrication of the Au nanowire patterns that underpin the NAVAC method for directing cell orientation is based on nanoskiving [19] as shown in **Figure 1a**. First, a polydimethylsiloxane (PDMS) grating is replicated into epoxy via soft lithography. Second, the successive deposition of gold (100 nm thickness) was performed at a glancing angle on the unilateral sides of the shaped epoxy replica and subsequently embedded again in epoxy. From this block 100 nm-thick slices were cut using an ultramicrotome and were allowed to float onto water. These nanowire-containing slices were transferred onto glass or gold substrates and manipulated to construct nanowire patterns with different angles (**Figure 1b/c**) [20]. The epoxy matrix was then removed by O_2 plasma etching leaving behind patterns of pristine, Au nanowires; width 105 nm $\pm$ 34 nm (defined by vapor deposition) and height 100 nm (defined by the slab thickness during sectioning) (**Figure 1d/e**). Scanning electron microscopy (SEM) of the Au nanowire patterns confirmed that the transfer processes does not damage the wires and that these can be positioned precisely to obtain ordered nanowire configurations (alignment, patterns (60 and 90º)) with spacing (10 μm) (**Figure 1b/c**).

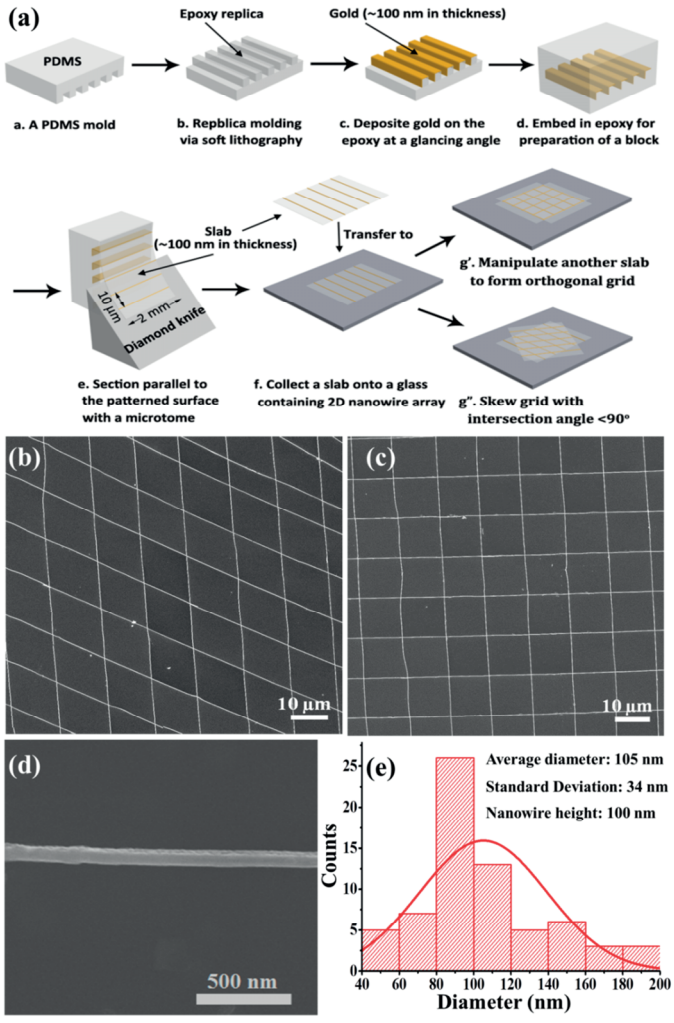

Figure 1. Fabrication and morphology of Au nanowire patterns. (a) Schematic representation of the Au nanowire patterns fabricated by nanoskiving. (b-d) SEM images of Au nanowires with an intersection angle of 60 and 90° as well as single nanowire morphology. (e) Statistical graph of nanowire diameter.

The Au nanowires were positioned with various directions (i.e., 0, 60, 70 and 90° nanopatterns) on the glass substrates for studying cell response. We refer to these substrata as follows: (i) 0° glass (parallel nanopatterns on glass), (ii) 60° glass (nanopatterns at a 60° angle on glass), (iii) 70 ° glass, (iv) 90° glass (a square pattern), and (v) 0° gold (parallel nanopatterns on gold). The pure glass and gold substrates were used as controls. No additional growth factors or adhesion molecules were added to the

medium to avoid any influence on cell adhesion and growth. Also, no additional surface modifications were performed on the substrates before cell seeding i.e. there was no addition of self-assembled monolayers, peptide functionalization or other forms of manipulation to direct cellular behavior. For the study, hBM-MSCs were selected as a model cell-type because they are known to be a representative physicochemical stimuli sensing cell type [4,10]. We characterized their attachment, organization as well as morphology to understand how the cells interact with the nanowire arrays. For oriented Au nanowire arrays on glass substrates, the cell bodies elongated to align along the direction of the nanowires (**Figure 2a**). Compared to unidirectional Au nanowires on glass, the Au nanowire assemblies with different angles on glass showed entirely different cellular behavior: (1) most of the cells displayed a vector response to the 60 and 70º patterns (**Figure 2b/c**); (2) they no longer sensed the vector on 90º pattern but the cells displayed a bimodal alignment responding either to the 0º or 90º nanowire orientation (**Figure 2d**). We found that when the angle of the nanowires on glass is increased from 0° to 90°, hBM-MSC arrangement shows a transition from a unidirectional distribution to the vector response to a bimodal polarization pattern. Additionally, hBM-MSC elongation decreased with increasing nanowire angles from 0 to 90º. For a better understanding of cell response on the different surfaces, cell vector response and elongation were determined by a quantitative analysis of the positively stained cells after 2 days culture on the nanowire-arrays. From **Figure 2e/f**, the degree of cell vector response and elongation decreased with increasing Au nanowire angles from 0 to 90º. Interestingly, when the angle increased from 0 to 60 degree, the average of cell vector response decreased 26 percent; When the angle increased from 60 to 70 degree, the average of cell vector response dropped 25 percent (**Figure 2e**). The results indicate that the attachment and arrangement of cells were strictly regulated by the various architectures of the nanowires on the glass substrate.

The characterization of cell alignment via NAVAC was complemented by investigations of the focal adhesion contacts and cytoskeleton because the formation of focal adhesion spots and filopodia as well as the cytoskeleton organization are the starting point of a chain of signaling events that lead to cell attachment, proliferation, motility/migration, and differentiation [16,21,22]. The focal adhesion formation and cytoskeleton organization on the respective surfaces were investigated with a triple-label fluorescence staining of the vinculin (focal adhesion protein), actin (cytoskeleton), and cell nucleus. Qualitative comparison of the cell behavior on the different patterns shows that more focal adhesion contacts are formed on the flat gold reference and 0º gold as compared to the flat glass control and 0º glass, while no obvious differences were observed between the Au nanowire surfaces with different patterns with respect to amount of focal adhesions (**Figure 2a-d, 3a-c, S1**). Moreover, a higher number of vinculin spots were observed on the Au nanowire surfaces as compared to the flat glass control. Based on observations of focal adhesion morphology on all surfaces, dash-like focal adhesions were observed on flat gold and Au nanowire surfaces, but dot-shaped structures were found on the flat glass control. These differences clearly indicate an altered cell adhesion as well as cell migration behavior induced by a different interaction with glass and gold as focal adhesions are important for both these processes. From a more detailed investigation of the cell border, a significantly higher number of filopodia were seen on all of the Au nanowire surfaces as compared to the bare glass and gold controls (**Figure 2a-d, 3a-c**). Gustafson *et al.* were the first to report filopodia in cells [22], which have been widely

recognized as one of the main sensors in cells and are associated with surface chemical and topographical sensing which are here most likely the moving edges of motile cells [16]. As depicted in high contrast images (**Figure S2**), cells were well-spread with many contracted and well-defined actin stress fibers on all surfaces.

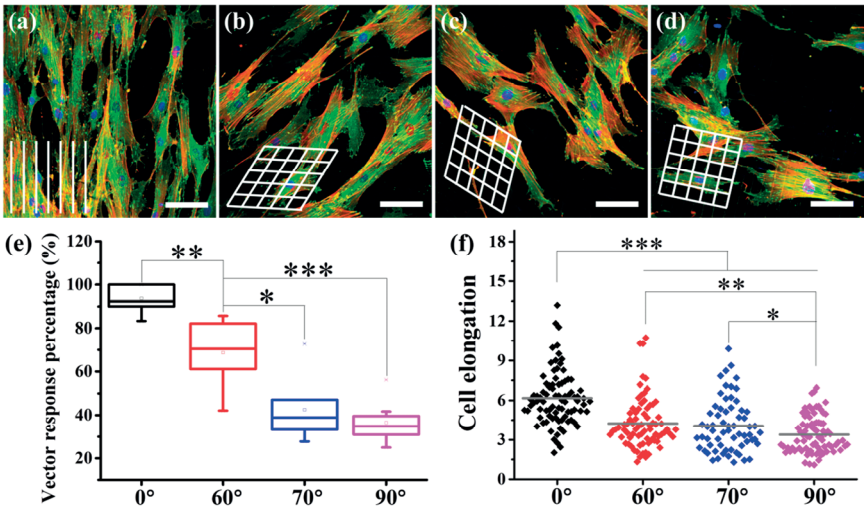

Figure 2. Cell vector response to biomimetic patterns of Au nanowires. Fluorescence images of hBM-MSCs on (a-d) Au nanowire-arrays on glass substrates with angles of (a) 0°, (b) 60°, (c) 70° and (d) 90°. Scale bars: 75 μm. Green staining is vinculin; Red staining is F-actin, visualized by TRITC-phalloidin staining and blue staining is nucleus, stained by DAPI. (e, f) Cell vector response percentage and cell elongation, respectively.

To explore how the nanowire arrays direct hBM-MSC behavior, we studied the controls (i.e., aligned Au nanowires on an Au substrate, planar glass and gold) and their protein adsorption. Compared to cell orientation on unidirectional Au nanowires on glass, cells were much less aligned along unidirectional Au nanowires on gold substrates (**Figure 2a/3a**). On pristine, planar glass and gold the cells oriented randomly (**Figure 3b/c**). The cell angle of alignment is defined as the angle between the major axis of the cell and the nanowire direction, ranging from 0 (a perfectly aligned cell) to 90° (a cell perpendicular to the nanowire direction). The average cell angle on flat glass and gold surfaces were found to be 46° and 41°, respectively, indicating no specific cell orientation. For hBM-MSCs cultured on the 0° gold substrate, the average of cell angle orientations was found to be 31°, which indicates a modest contribution from nanotopography effects caused by the nanowire structures. For this substrate, no difference in affinity is present between nanostructures and substrate as both are comprised of unmodified gold. In contrast, hBM-MSCs cultured on 0° glass showed an average cell angle of 4° (**Figure 3d**) which demonstrates that the nanotopography effects may be enhanced when cells respond differently toward different materials. The trend of cell alignment displays a positive correlation with respect to the focal adhesion

orientation (**Figure 3e**), which indicates that focal adhesion orientation may precede cell alignment and then result in the future cell extension or elongation.

Importantly, comparing cell adhesion on glass and unmodified gold surfaces reveals a large difference in cell adhesion capabilities determined from the cell density after 1.5 hours adhesion time and subsequent washing to remove all non-adhered cells. **Figure 3f/g** show significant differences in cell density and surface coverage between planar glass and gold surfaces ($p < 0.001$). The cell density on pristine, planar gold surfaces is 2.4 times higher than on glass and cell surface coverage is 2.6 times higher, suggesting that hBM-MSCs respond to and adhere faster to gold than to glass. There is no significant difference in the area per-cell (μm^2/cell) on glass or gold, however, we found significant differences for the area of single focal adhesions and their elongation on glass and gold surfaces ($p < 0.001$) (**Figure 3h/i**). The single focal adhesion area on planar gold was 2.2 times higher than that on glass. The degree of elongation of a focal adhesion provides a further indication of focal adhesion structural maturity and polarization. Collectively, these results indicate that cells prefer to adhere to unmodified gold rather than glass; therefore, the inherent difference in affinity between these two materials—without specific surface modification or the use of specialized coatings—contributes significantly to direct cell orientation. Therefore, the results indicate that cell vector response was induced specifically by combining a structured, high-affinity material (patterned gold) with a non-directional, low-affinity material (planar glass).

Further, we studied hBM-MSC affinity difference between gold and glass measuring their protein adsorption. As is known, under conventional culture conditions, cells never directly interact with the materials but also via a conditioning protein film that originates from the culture medium supplemented with fetal bovine serum (FBS) [23]. This adhesion is generally much faster than the cell adhesion events. To identify that the difference in protein adsorption is most likely the determining factor for the material affinity effect was determined by quartz crystal microbalance with dissipation (QCM-D). Protein adsorption behavior was on gold and glass surfaces was compared to provide a possible explanation for the cell adhesion difference. The adsorbed protein mass and thickness measured by QCM-D on the gold surface was much greater than on the silica surface: ~3735 versus ~2490 ng/cm^2, ~37 versus ~25 nm, respectively (**Figure 3j**). Cell adhesion is mediated through adsorbed proteins and proportional to the initial adsorbed protein mass. In addition, the initial protein adsorption rate on the gold and silica surfaces is comparable. However, during the secondary adsorption the rate of protein adsorption onto the gold surface (4.73 ng/s) is faster than that onto the silica surface (1.68 ng/s), most likely protein deformation and/or rearrangement on the surfaces is different [24–26]. These differences are likely due to two reasons: (1) surface wettability (gold: 62º; glass: 35º) as indicated in **Figure 3k**. The protein adsorption is dependent on the surface wettability. Protein adsorption increases with increasing of surface water contact angle, protein adsorption increases with higher surface hydrophobicity [27]. (2) surface charge (gold: neutral; glass: negative [28]). Proteins have different specific interactions on Au than on SiO_2. It is clear that BSA has a preference for binding to positively charged or neutral surfaces, because the isoelectric point of BSA is 4.6, and therefore BSA is negatively charged at pH 7.0 [29].

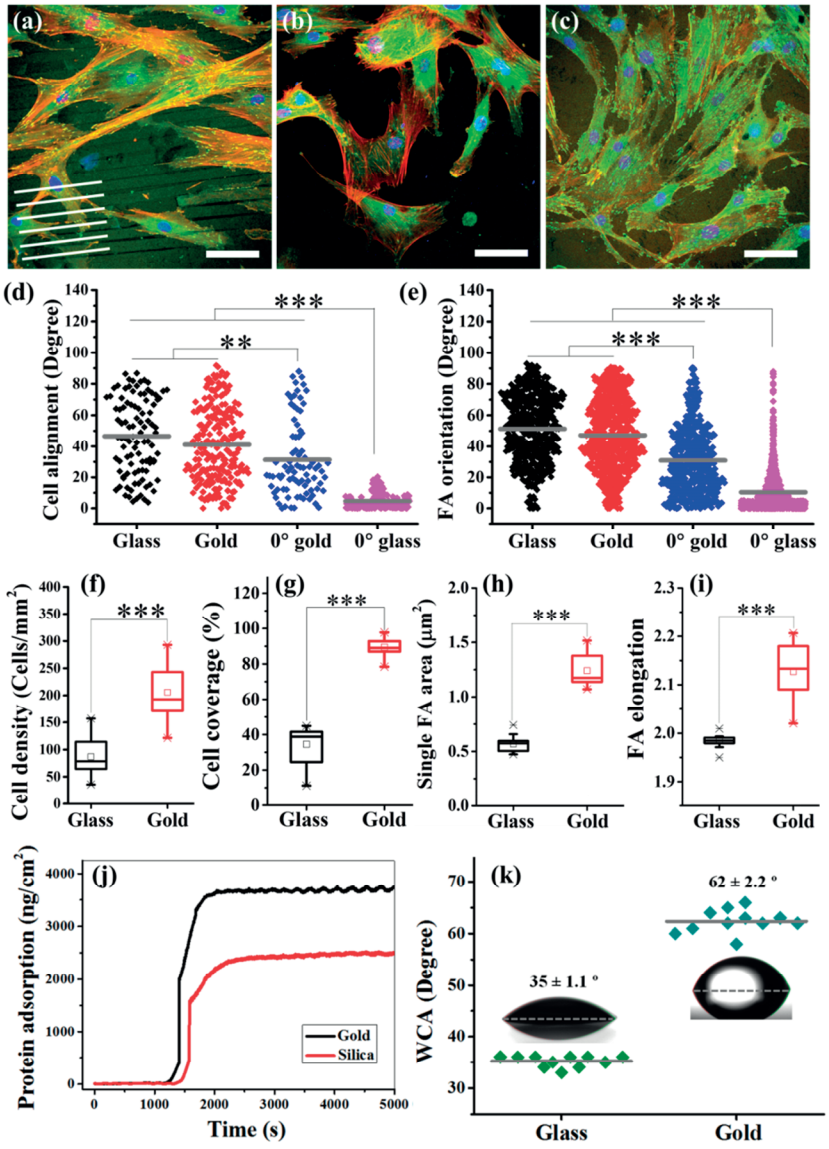

Figure 3. Fluorescence images of hBM-MSCs on (a) aligned Au nanowires on an Au substrate, (b) flat glass and (c) gold controls. Scale bars: 75 μm. Green staining is vinculin; Red staining is F-actin, visualized by TRITC-phalloidin staining and blue staining is nucleus, stained by DAPI. (d, e) Cell alignment and focal adhesion (FA) orientation, respectively. (f-i) Cell density, surface coverage, single FA area, and elongation on glass and gold controls after 2 days cultivation, respectively. (j) Protein adsorption profiles on gold and silica surfaces. (k) Water contact angle on gold and glass surfaces.

Stem cells are able to sense the external material features and respond to physicochemical cues via signal transduction pathway and thereby influencing cell behavior [6]. Herein, the adhesion and organization of hBM-MSCs are regulated by the orientation of the gold nanowire arrays which act as a non-invasive platform. The present study is aimed at examination of a critical transition of cell body from a unidirectional distribution to the vector response to an orthogonal polarization pattern induced by difference in protein adsorption caused by the inherent chemical and subcellular topographical cues. The polarization of cells was governed by two steps: the identification of underlying physicochemical anisotropy and subsequently the directional spreading in response to the guidance cues. The information communications between cell and the anisotropic nanobiointerface can activate the integrin-focal adhesion cytoskeleton actin transduction pathway, resulting in the stabilization and oriented growth of focal adhesions (**Figure 3e**) and sequentially generate contractile and aligned cytoskeleton actin (**Figure S2**). We found that the FAs and actin expression in the elongated hBM-MSCs guided by the nanowires differ from those on plain glass and gold surfaces. The cytoskeleton actin on the nanowires has more prominent stress fibers through the cell body with more and oriented FAs. On the non-structured surfaces, the hBM-MSCs display an unordered cytoskeleton actin in the cell body. Moreover, a slightly increased cell number and more elongation was found on the nanowires as compared to the flat substrates (**Figure 2 and 3**). These observations demonstrate that surface anisotropic physicochemical features can profoundly influence hBM-MSC organization (alignment and the vector response), spreading, the formation and orientation of FAs and cytoskeletal reorganization. These material properties include surface chemistry and (nano)topography and therefore play an important role whether a cell would preferentially adhere to a specific material [30,31]. It is logical to control material surface properties because of the highly complex, multicomponent and combinatorial cues present in the stem cell niche. Various material surface features in multiparameter and combinatorial fashions in the cellular microenvironment are increasingly considered as the critical role in stem cell behavioral decisions. This work therefore provides an ideal model and new insights into a deeper understanding of cell-nanobiointerface interactions.

3.3. CONCLUSION

In summary, the NAVAC approach for biomimetic nanotopographies achieves the precise control and patterning of nanostructures via nanoskiving, which is a simple and portable technique as well as compatible with a wide variety of materials. These nanostructures affect the orientation and growth of cells, enabling a powerful, simple and low-cost method to study the ECM and to recapitulate cell behaviors *in vitro*. Facile control over the biomimetic nanowire structures affords an interactive and effective method to regulate cell organization through the synergistic effects of surface nanotopography and chemical cues, enabling control over not only effective cell adhesion and orientation, but also the vector response of the cells. When the angle of the nanowires on glass was increased from 0° to 90°, hBM-MSC arrangement exhibited a transition from a unidirectional distribution to the vector response to a bimodal

polarization pattern. Among them, the degree of cell vector response and elongation decreased with increasing Au nanowire angles from 0 to 90º. The focal adhesion and filopodia as cellular sensors play an important role in cell organization; contact guidance and the scalability and ease of fabrication of NAVAC surfaces facilitate studies of these processes and the discovery and application of ordered arrays of cells that are otherwise not accessible. The initial findings reported herein will significantly contribute to the knowledge of the developmental biology of stem cells by fostering a frictionless interface between nanoscience, biochemistry, and cell biology. The excellent electrical and thermal conductivity of Au nanowires also creates an opportunity to explore neural tissue behavior or intracellular delivery of therapeutic macromolecules under electrical or thermal stimulation. Moreover, the surface chemistry of the substrate and the Au nanowire arrays can be modified to include functional groups or bioactive factors (protein) to study cell-surface interactions further.

3.4. EXPERIMENTAL SECTION

Preparation of Au nanowire arrays: The glass and silicon wafers used in this research were cleaned by piranha solution (H_2SO_4:H_2O_2=3:1). Further, the gold surface was formed by thermal evaporation of a gold film on silicon wafer in vacuo and cleaned with air plasma before use. The wafers were cut to the dimensions of 1 cm length × 1 cm width before collecting sections fabricated by nanoskiving from the boat of the diamond knife. Photoresist was spin-coated on silicon wafers at 3000 rpm to form a 2-μm thick layer which was then patterned to 5-μm stripes with 5-μm separation using photolithography. After the patterned silicon surface was passivated with trichloro-(1H, 1H, 2H, 2H-perfluorooctyl) silane (purchased from Aldrich), poly(dimethylsiloxane) (PDMS) (Dow Corning Sylgard 184, curing agent and prepolymer in 1:10 w/w ratio) was coated on the stripe mold and cured for 3 h at 60 ºC in an oven. Epofix epoxy prepolymer (prepolymer and harder in 15:2 in v/v ratio) was cured against the PDMS mold at 60 oC for 3 h to replicate the pattern in epoxy. Then a 100-nm thick layer of gold was deposited on the patterned epoxy substrate at a glancing angle of 45o. The gold-covered epoxy substrate was cut into small pieces that were embedded into more epoxy prepolymer to form epoxy blocks. A block was placed in the ultramicrotome (Leica EM UC-7) and trimmed to the width of the diamond knife (3 mm Diatome Ultra 35º). After alignment of the flat block face with the diamond knife edge, the block was sectioned to 100 nm at 1 mm/s to produce epoxy sections containing gold nanowire arrays in a plane parallel to the gold film. The sections were collected to a substrate (glass or gold). The epoxy resin was then removed by oxygen plasma. To prepare 3D gold nanowire arrays, one section was transferred and positioned onto another section with different intersection angle using an on-demand transfer approach that utilizes a film of polystyrene as carrier layer and aluminum as sacrificial layer.

SEM characterization: The gold nanowire nanostructures were observed by scanning electron microscopy (SEM) using JEOL FESEM 6700F electron microscope with electron energy of 3 kV.

Cell culture: Human bone marrow-derived mesenchymal stem cells (donor, Lonza™, passage 5) were used for the cell experiments. The growth medium consisted of Alpha modified Eagle medium (Gibco), 10% (v/v) fetal bovine serum (Gibco) and 0.1% (v/v) ascorbic acid 2-phosphate (Sigma). Cells were incubated at 37°C, 5% CO_2. The cells were harvested at approximately 80-90% confluence from T75 culture flasks by trypsin for 3-5 min at 37°C for further subcultures.

Cell adhesion studies: All samples (1.0 cm × 1.0 cm) were treated with 70% ethanol for sterilization and placed in 24-well plates for overnight. Afterwards, mesenchymal stem cells derived from human bone marrow (hBM-MSCs) were seeded onto the samples in 24-well plates at a density of 2 × 104 cells/well for cell adhesion. All samples were stored in an incubator at 37 °C and 5% CO_2. After 1.5 hours, non-adherent cells were removed, and 1 mL fresh growth medium was added in each well for two days culture. The low cell adhesion density and the short culture time ensure that cell-cell interactions, proliferation, and ECM deposition can be excluded as a variable. The hBM-MSCs were fixated with 3.7% paraformaldehyde (Sigma-Aldrich) in PBS for 20 min at room temperature, and subsequently washed 3 times with PBS. Afterward, the cell membrane was permeabilized with 0.5% TritonX-100 (Sigma-Aldrich) solution for 3 min. A 5% BSA in PBS solution was added for 30 min to block nonspecific binding. After withdrawing the BSA solution, the primary antibody against vinculin (clone hVin-1, Sigma, 1:100) was used in combination with a secondary FITC-labeled goat-anti-mouse antibody (Jackson Immunolab, 1:100). In addition, DAPI and TRITC-phalloidin were used to stain the cell nuclei and F-actin, respectively. Cells were observed using a LEICA TCS SP2 CLSM equipped with a 40 × NA 0.80 water immersion objective. The quantitative analysis of focal adhesion area and orientation was done by using Focal Adhesion Analysis Server [32] and ImageJ software was used to measure the cell average, area, orientation and elongation. A measurement of cell and focal adhesion elongation ranging from 1 (a perfect circle) to ∞ (a straight line), which was calculated as L/W (L=length, W=width).

Cell and focal adhesion orientation are determined by a fixed arbitrary direction on the planar substrates without nanowires. For the nanowire covered substrates, the orientation of the nanowire is depicted as 0° and cells or focal adhesions aligned perfectly to the wires have a 0° orientation. In addition, the vector response percentage is the number of cell vector response divided by the total cell number.

Quartz crystal microbalance with dissipation (QCM-D) measurement: QCM crystals were cleaned based on supplier's instructions. Gold coated crystals were washed in a 3:1:1 mixture of ammonia (28%), hydrogen peroxide (30%), and ultrapure water for 10 min at 75 °C, and then rinsed with ultrapure water and dried under nitrogen. Silica coated crystals were cleaned by 2% (w/v) sodium dodecyl sulphate (SDS) for 30 min, followed by submersion in ultrapure water and dried under nitrogen. As a final step, QCM crystals were put into a UV/ozone plasma for 20 min to remove molecular contaminants. Freshly cleaned crystals were left in ambient air for one week in order to have a similar starting conditions with the nanowires on glass used in the cell experiments.

QCM measurements were performed on a Q-Sense-E4 instrument (Q-Sense, Sweden) with dissipation. An initial baseline was established by flowing PBS buffer. Freshly prepared cell medium (Alpha modified Eagle medium (Gibco), 10% (v/v) fetal bovine serum (Gibco) and 0.1% (v/v) ascorbic acid 2-phosphate (Sigma)) was flowed to obtain the adsorption plateau and establish a final stable line. All QCM-D experiments were carried out at a temperature of 37 °C and a flow rate of 10 μL/min controlled by a peristaltic pump (Ismatec SA, Glattbrugg, Switzerland). The differences in frequency, ΔF, and dissipation factor, ΔD were used to calculate the protein adsorption. The mass of adsorbed protein was attained by fitting ΔF and ΔD to the Voigt model using Q-tools software package.

Water contact angle (WCA) measurement: To identify the wettability of gold and glass surfaces, the static WCA measurement was performed using the sessile drop method. Different droplets of MilliQ water were placed randomly at different locations on each sample (N = 3). The projected images of the droplets were analyzed for determining contact angles.

Statistical analysis: All data points are expressed as mean values ± standard deviation. Statistical analysis was performed using Origin 9.0 software. All the data was analyzed using one way analysis of variance (ANOVA) with Tukey's test to determine differences between groups. A value of $p < 0.05$ was considered to be statistically significant.

ACKNOWLEDGEMENTS

Q.H.Z. is very grateful for financial support of the China Scholarship Council (No. 201406630003). The authors thank Yafei Luan for fruitful discussions. Part of the work has been performed in the UMCG Microscopy and Imaging Center (UMIC), sponsored by NWO-grant 40-00506-98-9021.

SUPPORTING INFORMATION

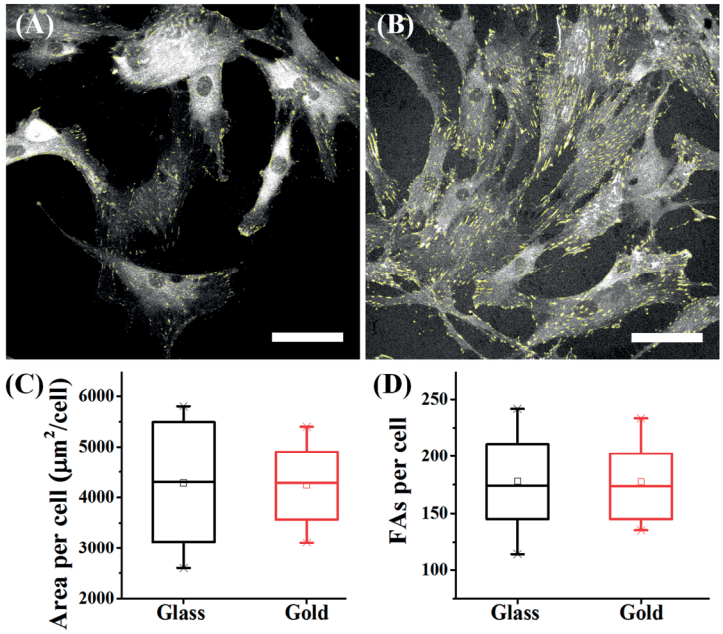

Figure S1. Cell response and focal adhesion (FA) formation on flat glass and gold controls. (A,B) The highlight of focal adhesion contact points for hBM-MSCs after 2 days cultivation. Scale bars: 75 μm. (C,D) Cell area and FAs per cell, respectively.

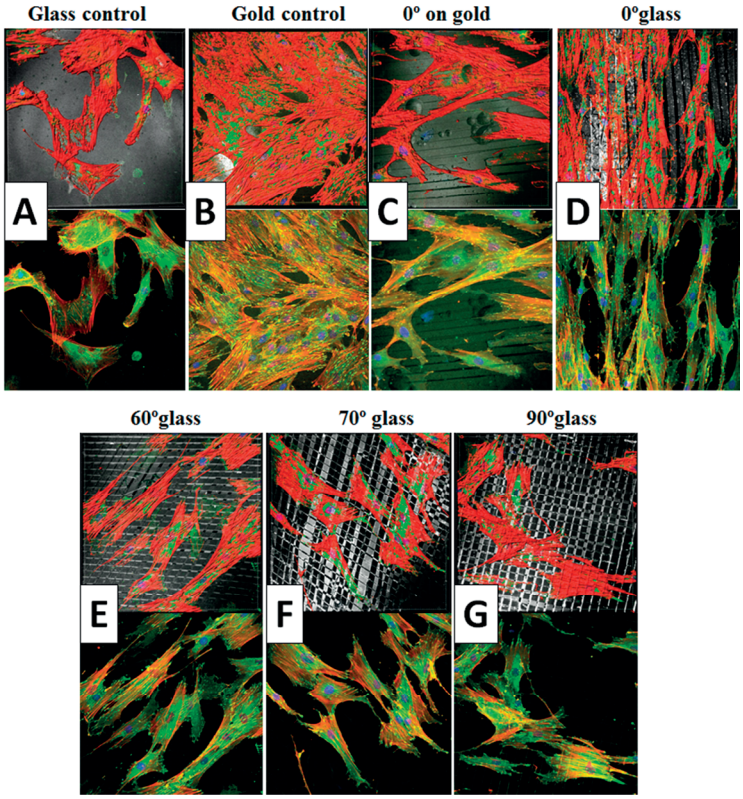

Figure S2. Cell response to biomimetic patterns of Au nanowires. Fluorescence images of hBM-MSCs with distinct actin fiber visible on top of (A) flat glass; (B) gold control; (C) aligned Au nanowires on a Au substrate. (D-G) Au nanowire-arrays on glass substrates with angles of (D) 0°; (E) 60°; (F) 70°; and (G) 90°. Green staining is vinculin; Red staining is F-actin, visualized by TRITC-phalloidin staining and blue staining is nucleus, stained by DAPI.

REFERENCES

[1] R. Langer, D. a Tirrell, *Nature* **2004**, *428*, 487.
[2] Q. Zhou, H. Zhang, Y. Zhou, Z. Yu, H. Yuan, B. Feng, P. van Rijn, Y. Zhang, *Macromol. Biosci.* **2017**, *17*, 1700268.
[3] J. Li, Y. Chen, Y. Yang, N. Kawazoe, G. Chen, *J. Mater. Chem. B* **2017**, *5*, 1353.
[4] A. M. Schaap-Oziemlak, P. T. Kühn, T. G. van Kooten, P. van Rijn, *RSC Adv.* **2014**, *4*, 53307.
[5] A. Sechi, J. M. G. Freitas, P. Wünnemann, A. Töpel, R. T. Paschoalin, S. Ullmann, R. Schröder, G. Aydin, S. Rütten, A. Böker, M. Zenke, A. Pich, *Adv. Mater. Interfaces* **2016**, *3*, 1600455.
[6] W.-G. Bae, J. Kim, Y.-H. Choung, Y. Chung, K. Y. Suh, C. Pang, J. H. Chung, H. E. Jeong, *Biomaterials* **2015**, *69*, 158.
[7] Z. Yin, X. Chen, J. L. Chen, W. L. Shen, T. M. H. Nguyen, L. Gao, H. W. Ouyang, *Biomaterials* **2010**, *31*, 2163.
[8] Q. Zhou, J. Xie, M. Bao, H. Yuan, Z. Ye, X. Lou, Y. Zhang, *J. Mater. Chem. B* **2015**, *3*, 4439.
[9] U. G. K. Wegst, H. Bai, E. Saiz, A. P. Tomsia, R. O. Ritchie, *Nat. Mater.* **2015**, *14*, 23.
[10] Q. Zhou, O. Castañeda Ocampo, C. Guimarães, P. Kuhn, T. van Kooten, P. van Rijn, *ACS Appl. Mater. Interfaces* **2017**, *9*, 31433.
[11] Q. Zhou, P. Wünnemann, P. T. Kühn, J. de Vries, M. Helmin, A. Böker, T. G. van Kooten, P. van Rijn, *Adv. Mater. Interfaces* **2016**, *3*, 1600275.
[12] M. R. Lee, K. W. Kwon, H. Jung, H. N. Kim, K. Y. Suh, K. Kim, K.-S. Kim, *Biomaterials* **2010**, *31*, 4360.
[13] H. Takahashi, M. Nakayama, K. Itoga, M. Yamato, T. Okano, *Biomacromolecules* **2011**, *12*, 1414.
[14] H. Takahashi, M. Nakayama, T. Shimizu, M. Yamato, T. Okano, *Biomaterials* **2011**, *32*, 8830.
[15] A. Wennerberg, T. Albrektsson, *Clin. Oral Implants Res.* **2009**, *20*, 172.
[16] M. J. Dalby, M. O. Riehle, H. Johnstone, S. Affrossman, A. S. G. Curtis, *Cell Biol. Int.* **2004**, *28*, 229.
[17] O. F. Zouani, C. Chanseau, B. Brouillaud, R. Bareille, F. Deliane, M.-P. Foulc, A. Mehdi, M.-C. Durrieu, *J Cell Sci* **2012**, *125*, 1217.
[18] L. Dong, K. Cheng, Y. Zhou, M. Yu, J. Gong, Y. Lin, Q. Luo, Q. Wang, W.-J. Weng, H. Wang, *ACS Appl. Mater. Interfaces* **2017**, *9*, 15274.
[19] P. Pourhossein, R. C. Chiechi, *ACS Nano* **2012**, *6*, 5566.
[20] Z. Zhao, Z. Zhou, G. Zhang, R. C. Chiechi, *Nanoscale Horizons* **2016**, *1*, 473.
[21] T. Shemesh, B. Geiger, A. D. Bershadsky, M. M. Kozlov, *Proc. Natl. Acad. Sci. U. S. A.* **2005**, *102*, 12383.
[22] L. Wolpert, T. Gustafson, *Exp. Cell Res.* **1961**, *25*, 311.
[23] A. E. Nel, L. Mädler, D. Velegol, T. Xia, E. M. V Hoek, P. Somasundaran, F. Klaessig, V. Castranova, M. Thompson, *Nat. Mater.* **2009**, *8*, 543.
[24] O. E. Castañeda Ocampo, P. Gordiichuk, S. Catarci, D. A. Gautier, A. Herrmann, R. C. Chiechi, *J. Am. Chem. Soc.* **2015**, *137*, 8419.
[25] H. Stadler, M. Mondon, C. Ziegler, *Anal. Bioanal. Chem.* **2003**, *375*, 53.
[26] J. L. Jordan, E. J. Fernandez, *Biotechnol. Bioeng.* **2008**, *101*, 837.
[27] P. Ying, G. Jin, Z. Tao, *Colloids surfaces B biointerfaces* **2004**, *33*, 259.
[28] S. H. Behrens, D. G. Grier, *J. Chem. Phys.* **2001**, *115*, 6716.
[29] S. Patil, A. Sandberg, E. Heckert, W. Self, S. Seal, *Biomaterials* **2007**, *28*, 4600.
[30] F. A. Denis, P. Hanarp, D. S. Sutherland, J. Gold, C. Mustin, P. G. Rouxhet, Y. F. Dufrêne, *Langmuir* **2002**, *18*, 819.
[31] Z. Zhang, Y. Fu, W. Yu, X. Qin, Z. Xue, Y. Liu, D. Luo, C. Yan, X. Sun, T. Wang, *Adv. Mater.* **2016**, *28*, 9589.
[32] M. E. Berginski, S. M. Gomez, *F1000Research* **2013**, *2*, 68.